Control Engineering Practice 109 (2021) 104725

Contents lists available at ScienceDirect

Control Engineering Practice

journal homepage: www.elsevier.com/locate/conengprac

Data-driven LPV model predictive control of a cold atmospheric plasma jet for biomaterials processing☆

Dogan Gidon [a], Hossam S. Abbas [b], Angelo D. Bonzanini [a], David B. Graves [a], Javad Mohammadpour Velni [c], Ali Mesbah [a,*]

[a] Department of Chemical and Biomolecular Engineering at the University of California, Berkeley, CA 94720, USA
[b] Institute for Electrical Engineering in Medicine, University of Lübeck, Lübeck, Germany
[c] School of Electrical and Computer Engineering at the University of Georgia, Athens, GA 30602, USA

ARTICLE INFO

Keywords:
LPV model identification
Predictive control
Atmospheric pressure plasma jets
Plasma processing

ABSTRACT

Cold atmospheric plasmas (CAPs) are increasingly used for treatment of complex surfaces in biomedical and biomaterials processing applications. However, the multivariable, distributed-parameter, and nonlinear nature of CAP dynamics and plasma–surface interactions, coupled with the sensitivity of plasmas to exogenous disturbances, make their safe, reproducible and effective operation challenging. This paper adopts a data-driven linear parameter-varying (LPV) modeling framework to learn a control-oriented model for predictive control of a kHz-excited atmospheric pressure plasma jet in Helium. A hierarchical model-based control strategy is proposed based on a supervisory LPV-based model predictive controller (LPV–MPC) to regulate the nonlinear thermal effects of plasma on a surface. Real-time control experiments demonstrate the effectiveness of the proposed LPV–MPC strategy for the multivariable control of surface temperature and plasma optical intensity, as well as for controlling the spatial delivery of the cumulative thermal effects of the plasma jet on a surface.

1. Introduction

Atmospheric pressure plasma jets (APPJs) are a class of cold atmospheric plasma devices that are capable of locally producing and delivering physical and chemical effects, including heat, electric fields, UV and visible range photons, ions, and short-lived reactive chemical species (Laroussi, Kong, Morfill, & Stolz, 2012), to complex surfaces. APPJs are increasingly used for surface processing and biomedical applications (Laroussi et al., 2012; Mani et al., 2015; Metelmann et al., 2018; Morent, 2013; von Woedtke, Metelmann, & Weltmann, 2014). However, reproducible and effective operation of APPJs suffers from challenges such as run-to-run variations (Shin & Raja, 2007), long time-scale drifts (Gerber et al., 2017), sharp spatial gradients in temperatures and reactive species concentrations (Arjunan, Obrusník, Jones, Zajíčková, & Ptasinska, 2016; Dünnbier, Schmidt-Bleker, Winter, Wolfram, Hippler, Weltmann, et al., 2013), and sensitivity to exogenous disturbances (e.g., changes in jet tip-to-surface separation distance, time-varying surface characteristics, ambient temperature, and humidity) (Breden & Raja, 2014; Gerling, Nastuta, Bussiahn, Kindel, & Weltmann, 2012; Norberg, Johnsen, & Kushner, 2015; Schmidt-Bleker, Winter, Bösel, Reuter, & Weltmann, 2016). Model-based control strategies have recently been shown to be indispensable to effective and reproducible operation of APPJs, particularly in safety-critical applications such as plasma medicine (Gidon, Curtis, Paulson, Graves, & Mesbah, 2018; Gidon, Graves, & Mesbah, 2017, 2019a; Keidar, Yan, & Sherman, 2019).

A major challenge in model-based control of APPJs arises from the multivariable and nonlinear nature of the plasma dynamics, as well as the poorly understood plasma interactions with complex surfaces (Mesbah & Graves, 2019). Much effort has been invested in the high-fidelity modeling and simulation of the behavior of cold atmospheric plasmas, mainly to better understand the complex behavior of the plasma and plasma–surface interactions (Lee et al., 2011; Van Dijk, Kroesen, & Bogaerts, 2009). However, high-fidelity plasma models are generally computationally expensive and therefore are not amenable to repeated simulations. The computational complexity of plasma simulations can further increase when incorporating surface effects of the plasma that may occur across multiple length- and time-scales (Bhoj & Kushner, 2006). Thus, high-fidelity plasma models are not suited for model-based controller design, particularly for optimization-based control strategies such as model predictive control (MPC) (Rawlings & Mayne, 2009) that rely on repeated model solution and optimization in real-time.

☆ This work was supported by the US National Science Foundation under Grants 1912757 and 1912772. The second author H. S. Abbas is funded by the Deutsche Forschungsgemeinschaft (DFG, German Research Foundation) under project 419290163.

* Corresponding author.
E-mail address: mesbah@berkeley.edu (A. Mesbah).

https://doi.org/10.1016/j.conengprac.2021.104725
Received 4 August 2020; Received in revised form 26 November 2020; Accepted 31 December 2020
Available online xxxx
0967-0661/

In Gidon et al. (2017), a lumped-parameter, physics-based model was used for control-oriented modeling and MPC of a radio-frequency APPJ in Argon. However, such simplified physics-based models typically depend on several assumptions that can be difficult to validate. In addition, it is often impractical to describe the complex interplay between chemical, physical and electrical effects of the plasma delivered to a surface using simplified physics-based models. Alternatively, purely data-driven modeling approaches such as subspace identification (Van Overschee & De Moor, 2012) have been shown to yield adequate descriptions of APPJs for multivariable control using MPC (Gidon et al., 2018). However, the main limitation of the resulting linear time-invariant (LTI) models stems from their inability to capture the inherently nonlinear dynamics of plasma and plasma–surface interactions. Thus, MPC strategies designed using LTI models can be effectively deployed only within a limited operating range of APPJs.

In this work, we adopt a purely data-driven approach in *linear parameter-varying* (LPV) framework (Mohammadpour & Scherer, 2012; Rugh & Shamma, 2000) for modeling and predictive control of a kHz-excited APPJ in Helium. LPV representations enable describing nonlinear and time-varying dynamics of complex systems in a (parametrized) linear setting. LPV models can be identified in state–space or input–output forms, the main feature of the latter being its capability to identify computationally efficient and yet highly accurate models by solving a low-complexity estimation problem using extensions of LTI-based approaches (Laurain, Gilson, Tóth, & Garnier, 2010). As such, LPV models are represented in terms of parametrized linear dynamics in which the model coefficients or state–space matrices depend on measurable parameters, called *scheduling variables* (Rugh & Shamma, 2000; Tóth, 2010). Thus, LPV models allow for the use of prevalent linear control synthesis tools for the design of model-based controllers for systems with nonlinear and time-varying behavior; see Mohammadpour and Scherer (2012) and references therein. Several successful applications have demonstrated the promise of LPV control in practice, see, e.g., Abbas, Ali, Hashemi, and Werner (2014), Bachnas, Tóth, Ludlage, and Mesbah (2014) and Mohammadpour and Scherer (2012). MPC strategies based on LPV model descriptions (LPV–MPC) have also developed into a popular approach for controlling nonlinear and time-varying systems (Abbas, Hanema, Tóth, Mohammadpour, & Meskin, 2018; Casavola, Famularo, & Franzé, 0000). However, designing LPV–MPC controllers critically hinge on identifying accurate LPV models. Hence, there has recently been increasing interest in data-driven LPV model identification approaches (Rizvi, Velni, Abbasi, Tóth, & Meskin, 2018; Tóth, 2010).

The main contribution of this paper lies in the identification of a data-driven LPV model for a kHz-excited APPJ in Helium and using the model for the design of a hierarchical model-based control strategy based on a supervisory LPV–MPC controller. The performance of this LPV–MPC strategy is demonstrated in real-time control experiments for two cases: (i) the multivariable control of surface temperature and plasma optical intensity in the presence of setpoint changes and disturbances in jet tip-to-surface separation distance; and (ii) the control of spatial delivery of the nonlinear thermal effects of a stationary APPJ, where a soft sensor is used for online estimation of the delivered thermal effects to the surface. The real-time control experiments reveal that the LPV–MPC strategy allows reproducible and effective operation of the APPJ over a relatively broad operating range of the APPJ, which is particularly useful for biomaterials processing applications.

This paper is organized as follows. Section 2 describes the experimental setup of the kHz-excited APPJ in Helium, as well as the plasma treatment objectives. Section 3 describes the proposed hierarchical model-based control strategy based on a supervisory LPV–MPC controller. Section 4 introduces the basic concepts and formulations of LPV modeling in input–output form and the LPV–MPC design. The performance of the proposed control strategy is demonstrated in real-time control experiments in Section 5.

2. Atmospheric pressure plasma treatment of complex surfaces

This section describes the APPJ setup that is used to collect data for LPV model identification and to conduct real-time control experiments. In addition, the control objectives for the two case studies considered in this work are described later in this section.

2.1. APPJ setup

The kHz-excited APPJ in Helium (He) shown in Fig. 1 is used for model identification and real-time control experiments. The details of this experimental setup are given in Gidon, Graves, and Mesbah (2019b) and briefly reviewed here. The APPJ consists of a copper ring electrode wrapped around a quartz tube, which serves both as a dielectric barrier and as the gas flow channel. A high alternating current (AC) voltage at a frequency of 20 kHz is applied to the electrode to achieve plasma ignition. The amplitude of the applied voltage is actuated via a custom-made function generator (XR-2206CP) interfaced with a micro-controller (Arduino UNO). The He flow rate is actuated via a mass flow controller (UFC-1200A), which is also interfaced with the micro-controller. A stepper motor attached to the quartz tube allows actuation along the vertical axis, thus enabling the manipulation of the jet tip-to-surface separation distance.

A fiber optic directed at the plasma–surface incident point collects the plasma optical emission intensity. A radiometric infrared thermal camera (Lepton FLIR 3) pointed at the surface is used to obtain spatially resolved measurements of surface temperature. AC-to-RMS converters (AD536A) allow embedded measurements of the plasma voltage and the current leaving the ground plate. These two measurements are used to compute applied power as $P_{\text{avg}} = V_{\text{rms}} I_{\text{rms}}$. The applied voltage is manipulated by an embedded proportional integral (PI) controller to maintain the applied power at a desired setpoint. Data acquisition and control are managed by a single board computer (Raspberry Pi 3) in Python. Data processing is performed in MATLAB using a conventional laptop, while the MPC algorithm is run in Python using the same laptop. The measurement and actuation signals between the laptop and the setup are exchanged over WiFi using TCP/IP communication protocol.

In summary, the APPJ setup can be thought of a system with two inputs and two outputs. The inputs are the He flow rate q and the power setpoint to the PI controller P^{set}, while the outputs are the spatially resolved surface temperature $T(x, y)$ and the plasma optical intensity I. Note that, depending on the control objective, one can extract the maximum surface temperature T_{max} instead of using the entire vector of the spatially resolved surface temperature.

2.2. Plasma treatment objectives

Safe and effective operation of APPJs requires control of instantaneous and cumulative effects of the plasma on the treated surface. These effects are often coupled and distributed across multiple time- and length-scales. The maximum surface temperature (T_{max}) is a key variable characterizing the thermal energy deposited on the surface by the plasma. On the other hand, plasma optical intensity (I) at the surface incident point is a proxy for the non-thermal effects of the plasma treatment, such as chemical effects. It is often desirable to maintain different combinations of maximum surface temperature and plasma optical intensity during the treatment via multivariable control (Gidon et al., 2018). However, these output variables are tightly coupled and exhibit nonlinear dynamics.

Furthermore, delivery of spatially distributed and cumulative effects of the plasma to the surface, i.e., “plasma dose”, is often one of the key objectives in the plasma treatment of complex surfaces. Generally speaking, plasma dose is intended to describe the nonlinear and non-decreasing nature of energy and/or species deposition on a surface (Gidon et al., 2017). Here, we focus on the delivery of spatially distributed *thermal dose*. We quantify the thermal dose using the metric

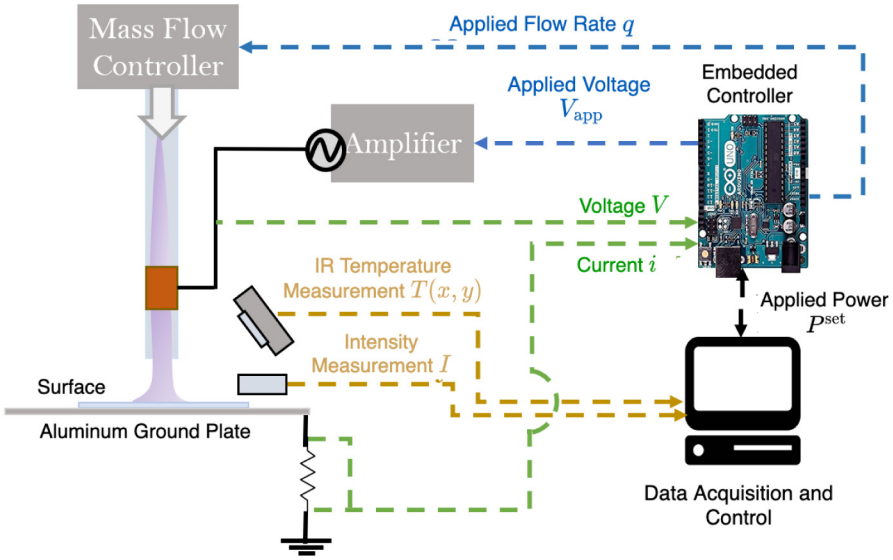

Fig. 1. Diagram of the experimental setup of the kHz-excited APPJ in He. The dashed arrows represent the flow of information, including the signals corresponding to the inputs (blue), embedded measurements (green), and slower time-scale measurements (brown). (For interpretation of the references to color in this figure legend, the reader is referred to the web version of this article.)

of cumulative equivalent minutes ($\mathrm{CEM_T}$), widely applied for dosing hyperthermia treatments (Dewhirst, Viglianti, Lora-Michiels, Hanson, & Hoopes, 2003), defined as

$$\mathrm{CEM_T} = \int_0^t K^{(43-T(\tau))}\,\mathrm{d}\tau, \tag{1}$$

where K is chosen to represent the thermal stress–response of the treated surface. In this work, K is given by

$$K = \begin{cases} 0 & T \le 39\ ^\circ\mathrm{C}, \\ 0.25 & 39\ ^\circ\mathrm{C} < T < 43\ ^\circ\mathrm{C}, \\ 0.5 & T \ge 43\ ^\circ\mathrm{C}, \end{cases} \tag{2}$$

which describes the temperature response of Chinese hamster ovary cells (Dewhirst et al., 2003).

A key observation in the thermal dose delivery using APPJs is that the spatial distribution of the surface temperature is radially symmetric (Gidon et al., 2019a, 2019b). Hence, a Gaussian parameterization can be used to approximate the surface temperature distribution as

$$T(r) = (T_{\max} - T_{\inf}) \exp\left(\frac{r^2}{\sigma^2(t)}\right) + T_{\inf}, \tag{3}$$

where $T_{\inf}$ is the ambient temperature, r is the radial distance from the centerline of the jet, and σ is the standard deviation of the distribution, which may change with time. The objective of the thermal dose delivery problem is then to maintain the width of the dose distribution (related to parameter σ) at the desired value while ensuring that the desired maximum dose (related to the maximum surface temperature at the jet centerline, $T_{\max}$) is delivered at the end of the treatment time (Gidon et al., 2019b). Moreover, constraints associated with practical operation considerations (e.g., patient safety and comfort during plasma treatment) should be respected. The control objectives considered in this paper are discussed in the next section.

3. Hierarchical control strategy based on LPV-MPC

We investigate two control problems for the kHz-excited APPJ in He. In Case I, we aim to achieve setpoint tracking for maximum surface temperature and plasma optical intensity in the presence of disturbances in jet tip-to-surface separation distance. To this end, a hierarchical control strategy is proposed (see Fig. 2), where an LPV–MPC controller is used in a supervisory capacity to compute the optimal power setpoint P^{set} and the He flow rate q that are applied to the

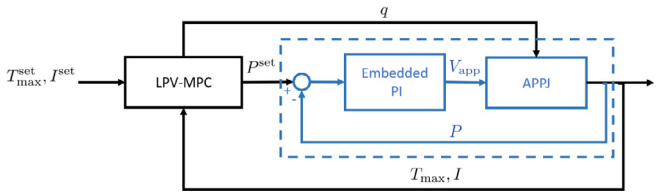

Fig. 2. Block diagram of the hierarchical control strategy for Case I. The control objective is to track setpoints for maximum surface temperature $T^{\mathrm{set}}_{\max}$ and plasma optical intensity I^{set}. The LPV–MPC controller computes optimal setpoint for the embedded power controller P^{set} and the optimal He flow rate q.

APPJ using a basic PI control layer. The He flow rate setpoint is sent to the mass flow controller, whereas the power setpoint is sent to an embedded PI controller that adjusts the power delivered to the APPJ. In Fig. 2, the inner loop, depicted by the dashed lines, shows the embedded PI controller used to maintain the plasma power at its setpoint by manipulating the applied voltage V_{app}. The formulation of the LPV–MPC problem is discussed in Section 4.

In Case II, we aim to control spatial thermal dose delivery to a surface using a stationary APPJ. The block diagram of the hierarchical control strategy is shown in Fig. 3. The key difference between Case I and Case II is the use of a *soft sensor*, which allows converting the cumulative dose reference $\mathrm{CEM}^{\mathrm{ref}}_{\mathrm{T}}$ to an instantaneous temperature setpoint $T^{\mathrm{set}}_{\max}$. The soft sensing strategy relies on inferring the desired rate (i.e., derivative) of dose delivery. With dose delivery rate defined, it is possible to invert the dose metric at every sampling instant to algebraically obtain the corresponding maximum temperature setpoint (Arora, Skliar, & Roemer, 2005). Given the dose accumulated in time instant k, $\mathrm{CEM}_{\mathrm{T},k}$, the linear rate of the dose delivery to achieve a desired final dose $\mathrm{CEM}^{\mathrm{ref}}_{\mathrm{T}}$ at the end of operation t_f is computed as

$$\alpha_k = \frac{\mathrm{CEM}^{\mathrm{ref}}_{\mathrm{T}} - \mathrm{CEM}_{\mathrm{T},k}}{t_f - t_k}. \tag{4}$$

The reference thermal dose for the next time point given the linear dose delivery rate can then be computed from

$$\mathrm{CEM}^{\mathrm{ref}}_{\mathrm{T},k} = \mathrm{CEM}_{\mathrm{T},k} + \alpha_k[t_{k+1} - t_k]. \tag{5}$$

The maximum temperature setpoint $T^{\mathrm{set}}_{\max,k}$ corresponding to the desired increase in dose can be computed by inverting the dose metric (1),

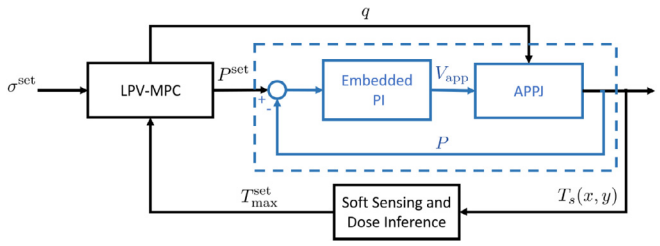

Fig. 3. Block diagram of the hierarchical control strategy for Case II. The control objective is to track setpoints for the standard deviation of surface temperature distribution σ^{set} and maximum surface temperature $T^{\text{set}}_{\text{max}}$ computed by the soft sensor. The LPV–MPC controller computes the optimal setpoint for the embedded power controller P^{set} and the optimal He flow rate q.

resulting in

$$T^{\text{set}}_{\text{max},k} = \begin{cases} \mathcal{M}(\text{CEM}^{\text{ref}}_{\text{T},k} - \text{CEM}_{\text{T},k}) & \alpha_k \geq 0 \\ 30°\text{C} & \text{otherwise,} \end{cases} \tag{6}$$

where the function $\mathcal{M}(\cdot)$ denotes the inverse of the dose metric function. Since the inverse of the dose metric is not real-valued when α_k is negative (i.e., the delivered dose exceeds the reference), $T^{\text{set}}_{\text{max},k}$ is set to its lower bound.

4. LPV-based model identification and predictive control design

This section discusses the data-driven LPV model identification in input–output form, followed by conversion of the input–output model to a state–space LPV model, which is then used to formulate the LPV–MPC problem.

4.1. LPV model identification in input–output form

An LPV input–output (IO) representation can be described in difference equation form by

$$y(k) = -\sum_{i=1}^{n_{\text{a}}} a_i(p(k))y(k-i) + \sum_{j=0}^{n_{\text{b}}} b_j(p(k))u(k-j) + w(k), \tag{7}$$

where $u(k) : \mathbb{Z} \to \mathbb{R}^{n_{\text{u}}}$, $y(k) : \mathbb{Z} \to \mathbb{R}^{n_{\text{y}}}$ and $p(k) : \mathbb{Z} \to \mathbb{P} \subset \mathbb{R}^{n_{\text{p}}}$ are, respectively, the input, output and scheduling variable vectors at a discrete-time instant k, $w(k)$ represents an additive disturbance vector, a_i, b_j are matrix functions of p with appropriate dimensions that are bounded within the parameter set $\mathbb{P}$

$$\mathbb{P} := \{p \in \mathbb{R}^{n_{\text{p}}} \mid p_{i,\min} \leq p_i \leq p_{i,\max},\ i = 1, 2, \dots, n_{\text{p}}\}.$$

The parameter set is assumed to be convex. n_{a} in (7) denotes the system order such that $n_{\text{a}} \geq n_{\text{b}} \geq 0$.

The LPV representation in (7) enables identification of low-complexity and yet reasonably accurate LPV descriptions of nonlinear and time-varying systems under practical assumptions on the disturbances and measurement noise (e.g., Laurain et al., 2010). An important step in *parametric-based* LPV model identification is the parameterization of the coefficients a_i and b_j (Tóth, 2010). Assuming that p is scalar, one simple approach is to consider polynomial functions as follows

$$c(p) = c_0 + c_1 p + c_2 p^2 + \cdots, \tag{8}$$

where $\{c_0, c_1, \dots\}$ are constants with appropriate dimension according to a_i, b_j and the number of the scheduling variables (note that c is used here as a proxy for model coefficients a and b in (7)). The constants in (8) constitute the parameters that should be estimated in LPV model identification. Note that, instead of polynomials, other basis functions can also be considered for the parameterization of the coefficients a_i and b_j, with potentially nonlinear dependence on the parameters p (see Tóth, 2010).

In order to use linear regression for estimation of the constants in (8), an autoregressive with exogenous input (ARX) model structure (Ljung, 1999) is commonly used, which implies that the disturbance $w(k)$ in (7) is assumed to be a zero-mean, discrete-time white noise process with a normal distribution. Accordingly, the LPV model identification problem can be formulated as a least-squares estimation problem, which can be solved efficiently. For multi-input multi-output (MIMO) LPV models, one model is typically identified for each output to simplify the identification problem. Thus, the MIMO LPV model is effectively described by a collection of multi-input single-output (MISO) models. For each MISO model, a_i is a scalar and b_j is a (row) vector corresponding to the number of inputs n_{u} in (7).

Based on the ARX model structure considered in this work, the predictor of (7) is formulated for the MISO case in the linear regression form as

$$\hat{y}(k) = \phi(k)^{\top}\theta, \quad \phi(k) = \varphi(k) \otimes \eta(k), \tag{9}$$

where $\theta = \left[c_0^{\top}, c_1^{\top}, \dots\right]^{\top}$ for both a_i and b_j, $\otimes$ denotes the Kronecker product, $\varphi(k)$ is the regressor vector given by

$$\varphi(k) = [-y(k-1)\ -y(k-2)\ \cdots\ -y(k-n_{\text{a}})\ u(k-1)^{\top}\ u(k-2)^{\top}\ \cdots\ u(k-n_{\text{b}})^{\top}]^{\top}, \tag{10}$$

and

$$\eta(k) = [1\ f_1(p(k))\ f_2(p(k))\ \cdots]^{\top}, \tag{11}$$

with $f_i(\cdot) : \mathbb{R}^{n_{\text{p}}} \to \mathbb{R}$ being continuous basis functions that can capture nonlinear dependence on p. Note that dependence on shifted versions of p in time, i.e., $\{\cdots, p(k-1), p(k), p(k+1), \dots\}$, (referred to as dynamic dependence Tóth, Abbas, & Werner, 2012) can also be considered in $\eta(k)$, which is the most general form of scheduling functions. The representation in (9) allows using the prediction error system identification method (Ljung, 1999), which employs least-squares estimation to obtain θ as follows

$$\theta = (\boldsymbol{\Phi}^{\top}\boldsymbol{\Phi})^{-1}\boldsymbol{\Phi}^{\top}Y, \tag{12}$$

where

$$Y = [y(1)\ y(2)\ \cdots\ y(N_{\text{d}})]^{\top}$$

and

$$\boldsymbol{\Phi} = [\phi(1)^{\top}\ \phi(2)^{\top}\ \cdots\ \phi(N_{\text{d}})^{\top}]^{\top},$$

with N_{d} denoting the number of data samples.

The MISO LPV models can be represented in a state–space form for the control design purposes, as discussed next.

4.2. Conversion of input–output LPV model to state–space LPV form

In order to design LPV–MPC controllers for the APPJ system, the identified LPV-IO models are transformed into an LPV state–space (SS) form. In general, transforming LPV-IO models to LPV-SS form, or vice versa, results in the so-called dynamic dependence since the transformed model would depend on time-shifted versions of the scheduling variable(s) (Tóth et al., 2012). The presence of dynamic dependence leads to difficulties in terms of controller design and implementation, as it could lead to dependence on future samples of the scheduling variables. To this end, we employ the augmented state–space form for converting the identified LPV-IO models by considering the dependence on $p(k-2)$ in (7). This allows deriving an augmented equivalent LPV-SS representation in a straightforward manner as follows.

We rewrite the identified LPV-IO model as

$$\begin{aligned}\hat{y}(k) = &-a_1(p_{k-2})\hat{y}(k-1) - a_2(p_{k-2})\hat{y}(k-2) - \cdots - a_{n_{\text{a}}}(p_{k-2})\hat{y}(k-n_{\text{a}}) \\ &+b_1(p_{k-2})u(k-1) + b_2(p_{k-2})u(k-2) + \cdots\end{aligned}$$

$$+b_{n_b}(p_{k-2})u(k-n_b). \tag{13}$$

MIMO LPV-IO models are constructed with coefficients a_i being diagonal matrices. Therefore, we can convert the MIMO models of the special form (13) of dynamic dependence by first multiplying both sides of (13) by the forward time shift operator, which yields

$$\begin{aligned}\hat{y}(k+1) = & -a_1(p_{k-1})\hat{y}(k) - a_2(p_{k-1})\hat{y}(k-1) - \cdots - a_{n_a}(p_{k-1})\hat{y}(k-n_a+1)\\ & +b_1(p_{k-1})u(k) + b_2(p_{k-1})u(k-1) + \cdots\\ & +b_{n_b}(p_{k-1})u(k-n_b+1).\end{aligned} \tag{14}$$

Note that in (14) the dependence is on p_{k-1} instead of p_{k-2}. To achieve offset-free control, we define $\Delta u(k) = u(k) - u(k-1)$. Substituting this into the above equation gives

$$\begin{aligned}\hat{y}(k+1) = & -a_1(p_{k-1})\hat{y}(k) - a_2(p_{k-1})\hat{y}(k-1) - \cdots - a_{n_a}(p_{k-1})\hat{y}(k-n_a+1)\\ & +b_1(p_{k-1})\Delta u(k) + \big(b_1(p_{k-1}) + b_2(p_{k-1})\big)u(k-1) + \cdots\\ & +b_{n_b}(p_{k-1})u(k-n_b+1).\end{aligned}$$

Next, we introduce the augmented state vector

$$\begin{aligned}&x(k)\\ &= \begin{bmatrix}\hat{y}^\top(k) & \hat{y}^\top(k-1) & \cdots & \hat{y}^\top(k-n_a+1) & u^\top(k-1) & \cdots & u^\top(k-n_b+1)\end{bmatrix}^\top,\end{aligned} \tag{15}$$

where $x \in \mathbb{R}^{n_x}$ with $n_x = n_y n_a + n_u(n_b-1)$. This leads to an augmented LPV-SS model in the form of

$$x(k+1) = A(p_{k-1})x(k) + B(p_{k-1})\Delta u(k) \tag{16a}$$

$$\hat{y}(k) = Cx(k), \tag{16b}$$

where

$$A(p_{k-1}) = \begin{bmatrix} -a_1 & \cdots & -a_{n_a-1} & -a_{n_a} & (b_1+b_2) & \cdots & b_{n_b-1} & b_{n_b}\\ I_{n_y} & 0 & \cdots & \cdots & \cdots & \cdots & \cdots & 0\\ \vdots & \ddots & \ddots & \ddots & \ddots & \ddots & \ddots & \vdots\\ 0 & \cdots & I_{n_y} & 0 & 0 & 0 & \cdots & 0\\ 0 & \cdots & 0 & 0 & I_{n_u} & 0 & \cdots & 0\\ 0 & \cdots & 0 & 0 & I_{n_u} & 0 & \cdots & 0\\ \vdots & \ddots & \ddots & \ddots & \ddots & \ddots & \ddots & \vdots\\ 0 & \cdots & \cdots & \cdots & \cdots & 0 & I_{n_u} & 0 \end{bmatrix},$$

$$B(p_{k-1}) = \begin{bmatrix} b_1\\ 0\\ \vdots\\ 0\\ I_{n_u}\\ 0\\ \vdots\\ 0 \end{bmatrix}, \quad \text{and} \quad C = \begin{bmatrix} I_{n_y} & 0 & \cdots & \cdots & \cdots & \cdots & \cdots & 0 \end{bmatrix}.$$

Note that the representation of the matrices $A(p_{k-1})$ and $B(p_{k-1})$ is simplified by dropping the dependence of a_i, b_j on p_{k-1}.

Remark 1. In this work, the system inputs are also the scheduling variables. Since the system inputs are computed by the control algorithm at every time instant k, they introduce a nonlinear interdependence that can make the control problem very slow, or even intractable. Therefore, we use the inputs at time k to schedule the control system at the next time instant $k+1$. The interdependence is thus circumvented because of the chosen dynamic dependence, which resulted in the dependence of the LPV-SS model (16) on $p(k-1)$.

The predictions of the LPV-SS model (16) over a prediction horizon N as a function of the measured state $x(k)$ and incremental inputs $\Delta U(k)$ can be compactly written as

$$X(k) = \mathcal{A}(k)x(k) + \mathcal{B}(k)\Delta U(k) \tag{17a}$$

$$Y(k) = \mathcal{C}(k)X(k), \tag{17b}$$

where

$$\begin{aligned} X(k) &= \begin{bmatrix}x(k)^\top & x(k+1)^\top & x(k+2)^\top & \cdots & x(k+N)^\top\end{bmatrix}^\top,\\ Y(k) &= \begin{bmatrix}\hat{y}(k)^\top & \hat{y}(k+1)^\top & \hat{y}(k+2)^\top & \cdots & \hat{y}(k+N)^\top\end{bmatrix}^\top,\\ \Delta U(k) &= \begin{bmatrix}\Delta u(k)^\top & \Delta u(k+1)^\top & \cdots & \Delta u(k+N-1)^\top\end{bmatrix}^\top,\\ \mathcal{A}(k) &= \begin{bmatrix} I\\ A\\ A^2\\ \vdots\\ A^N \end{bmatrix}, \quad \mathcal{B}(k) = \begin{bmatrix} 0 & 0 & \cdots & 0\\ B & 0 & \cdots & 0\\ AB & B & \cdots & 0\\ \vdots & \vdots & \ddots & \vdots\\ A^{N-1}B & A^{N-2}B & \cdots & B \end{bmatrix},\\ \mathcal{C}(k) &= \operatorname{diag}([C, \ldots, C]). \end{aligned}$$

Note that the system matrices A, B and C are dependent on the scheduling variables and thus must be updated at every sampling time k once the scheduling variable $p(k-1)$ becomes available. Here, it is assumed that the scheduling variable is fixed over the prediction horizon. The control inputs $U(k) = \begin{bmatrix}u(k)^\top & u(k+1)^\top & \cdots & u(k+N-1)^\top\end{bmatrix}^\top$ can be updated at each sampling time k by

$$U(k) = \Upsilon u(k-1) + \Pi \Delta U(k), \tag{18}$$

where

$$\Upsilon = \begin{bmatrix} I_{n_u}\\ I_{n_u}\\ \vdots\\ I_{n_u} \end{bmatrix}, \quad \Pi = \begin{bmatrix} I_{n_u} & 0 & \cdots & 0\\ I_{n_u} & I_{n_u} & \cdots & 0\\ \vdots & \vdots & \ddots & \vdots\\ I_{n_u} & I_{n_u} & \cdots & I_{n_u} \end{bmatrix}.$$

4.3. LPV-MPC problem formulation

The compact representation of the LPV-SS model over the prediction horizon N, i.e., (17), can now be used to formulate the LPV–MPC problem. At every sampling time k, the LPV–MPC entails online solution of the following optimal control problem

$$\min_{\Delta U(k)} \ \|Y_{\text{set}}(k) - Y(k)\|_{\mathcal{Q}}^2 + \|\Delta U(k)\|_{\mathcal{R}}^2 \tag{19a}$$

$$\text{s.t. } X(k) = \mathcal{A}(k)x(k) + \mathcal{B}(k)\Delta U(k), \tag{19b}$$

$$Y(k) = \mathcal{C}(k)X(k), \tag{19c}$$

$$\Delta U_{\min} \le \Delta U(k) \le \Delta U_{\max}, \tag{19d}$$

$$Y_{\min} \le Y(k) \le Y_{\max}, \tag{19e}$$

$$u_{\min} \le U(k) \le u_{\max}, \tag{19f}$$

$$\begin{aligned} x(k) = \big[&y^\top(k),\ y^\top(k-1),\ \cdots, y^\top(k-n_a+1),\\ &u^\top(k-1),\ \cdots,\ u^\top(k-n_b+1),\ \big]^\top, \end{aligned} \tag{19g}$$

where $\Delta U(k)$ constitutes the decision variables of the optimization (the prediction horizon N is assumed to be equal to the control horizon for notational convenience); $Y_{\text{set}}(k) = \big[y_{\text{set}}(k+1)^\top y_{\text{set}}(k+2)^\top \cdots y_{\text{set}}(k+N)^\top\big]$ denotes the output setpoints over the prediction horizon; $\mathcal{Q}(k) = \operatorname{diag}([\mathrm{Q}, \ldots, \mathrm{Q}])$ and $\mathcal{R}(k) = \operatorname{diag}([\mathrm{R}, \ldots, \mathrm{R}])$, with $\mathrm{Q} \succeq 0$, $\mathrm{R} \succ 0$ being weight matrices with appropriate dimensions; and the subscripts min and max denote the lower and upper bounds of the input and output constraints with appropriate dimensions. The optimal control problem (19) is implemented in a receding-horizon fashion, whereby the optimization problem is solved at each sampling time k to obtain an optimal sequence of control inputs $\Delta U^*(k) = \big[\Delta u^*(k)^\top \Delta u^*(k+1)^\top \cdots \Delta u^*(k+N-1)^\top\big]$. Then, the first optimal value of the sequence, i.e., $\Delta u^*(k)$, is applied to the system as $u^*(k) = \Delta u^*(k) + u^*(k-1)$.

Remark 2. Model predictions in the LPV–MPC depend on the future values of the scheduling parameters, which are usually not available in advance. A practical approach is to assume a constant value for the scheduling parameters over the prediction horizon. This way, the online optimization problem can be cast as a quadratic programming problem, as shown in the Appendix.

5. Experimental results

In this section, we first describe the data-driven LPV model identification for the kHz-excited APPJ in He, which is shown in Fig. 1. We then discuss real-time control implementations of the LPV–MPC hierarchical control strategies presented in Section 3.

5.1. LPV model identification and validation

Based on the control objectives specified in Section 3, we identify two MIMO LPV models using the inputs/outputs data collected from the APPJ. The controlled outputs of the first model are the maximum surface temperature T_{max} and plasma optical intensity I (Case I), whereas the controlled outputs of the second model are T_{max} and the standard deviation of the surface temperature distribution σ (Case II). The manipulated input variables of both models include the gas flow rate q and the embedded power set P_{set} (see Section 2). We identify a separate model for each controlled output as a multiple-input single-output (MISO) system, where a_i is a scalar and b_j is a 1×2 vector, since $n_u = 2$ and $n_y = 1$ in (7). This enables straightforward conversion of the MIMO LPV model to the state–space form, as discussed in Section 4.2.

The two manipulated variables are chosen as the scheduling variables of the LPV-IO models due to their direct effect on the system outputs and thus the operating region. We consider two cases for the LPV model identification: using a single scheduling parameter P_{set} and using two scheduling variables P_{set} and q. Furthermore, the coefficients a_i and b_j are considered to be dependent on $p(k-2)$ in (7), instead of $p(k)$, to avoid dependence of future outputs on future values of p when the identified LPV-IO models are converted into the state–space form for the MPC design. In addition, the coefficients a_i and b_j are parametrized with polynomial basis functions, as in (8), whose order ranges from third to fifth order.

To obtain low complexity models that are amenable to real-time computations while at the same time can adequately fit the given input–output data, we chose the order in (7) as $n_a = n_b = 2$ for modeling T_{max} and I; and $n_a = n_b = 3$ for modeling σ. It was observed that increasing the order did not result in significant improvement in the quality of models. Furthermore, for the MISO LPV-IO models of T_{max} and I, we considered one sample delay in both input channels, which implies $b_0 = 0$ in (7). For the MISO LPV-IO model of σ, we considered two sample delays in q, i.e., $b_0 = b_1 = 0$, and one sample delay in P_{set}.

Based on the ARX structure considered in this work, we formulated the predictor (7) for each MISO model in the linear regression form (9), with the regressor vector (10) and $\eta(k)$ given by (11), where $p(k-2)$ is replaced by $p(k)$. This allows for using the scheduling parameters as the control inputs in the LPV–MPC problem. The design of sufficiently rich input signals is crucial for a proper excitation of the important modes of the system for model identification. The excitation signals used here are shown in Fig. 4. These signals are chosen to cover various input combinations of interest, whose order is subsequently shuffled. Since the APPJ system is stable, the excitation experiments and the data collection were conducted in open loop.

To examine the quality of the identified LPV-IO models, the best fit rate (BFR) criterion, a.k.a. fit score, is used (Ljung, 1999)

$$\text{BFR} = 100\% \max\left(1 - \frac{\|y(k) - \hat{y}(k)\|_2}{\|y(k) - y_m\|_2}, 0\right),$$

where y_m is the mean of y and $\|\cdot\|_2$ denotes the ℓ_2 norm. We assessed the quality of the identified models using an independent dataset. The

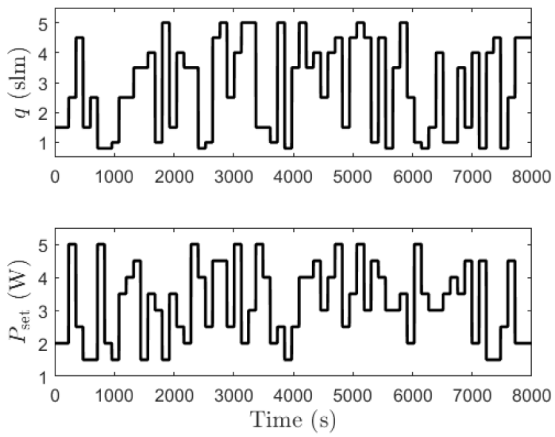

Fig. 4. Input signals used for exciting the kHz-excited APPJ in He to generate data for input–output LPV model identification.

Table 1
Structure of the input–output LPV models with two scheduling variables.

Output	n_a, n_b	Delay in samples	Polynomial order
T_{max}	2, 2	1	3
I	2, 2	1	3
σ	3, 3	2 in q, 1 in P_{set}	5

model predictions for the outputs T_{max} and I are superimposed with the validation data and are shown in Fig. 5. It is apparent that the predictions of the LPV model with two scheduling variables (Fig. 5(b)) outperform the predictions of the LPV model with a single scheduling variable (Fig. 5(a)). For the LPV models with two scheduling variables, the BFRs of T_{max} and I are 79.74% and 70.27%, respectively. For the LPV models with a single scheduling variable, on the other hand, the BFRs of T_{max} and I are 75.58% and 67.83%, respectively. For the prediction of σ, we only considered an LPV model with two scheduling variables. The predictions of σ along with the validation data are shown in Fig. 6. The BFR of σ is 57.27%, which indicates lower prediction accuracy compared to the other outputs. However, such prediction capability is adequate for the purpose of LPV controller design, as shown in the next section. Specifically, we accept the relatively low value of BFR for σ because σ is only used for controlling the width of the distribution of the delivered thermal dose; the surface temperature that has a BFR of 79.74% is the most important variable to control (see Fig. 9). Table 1 summarizes the structures of the LPV-IO models that are used for the design of the LPV–MPC controllers. For more clarity, the structure of the matrices $a_i(.)$ and $b_j(.)$ in (7) for the identified 2-input/3-output model are

$$a_1 = \begin{bmatrix} \bar{a}_1^{11} & 0 & 0 \\ 0 & \bar{a}_1^{22} & 0 \\ 0 & 0 & \bar{a}_1^{33} \end{bmatrix}, \quad a_2 = \begin{bmatrix} \bar{a}_2^{11} & 0 & 0 \\ 0 & \bar{a}_2^{22} & 0 \\ 0 & 0 & \bar{a}_2^{33} \end{bmatrix}, \quad a_3 = \begin{bmatrix} 0 & 0 & 0 \\ 0 & 0 & 0 \\ 0 & 0 & \bar{a}_1^{33} \end{bmatrix},$$

$$b_1 = \begin{bmatrix} \bar{b}_1^{11} & \bar{b}_1^{12} \\ \bar{b}_1^{21} & \bar{b}_1^{22} \\ 0 & \bar{b}_1^{32} \end{bmatrix}, \quad b_2 = \begin{bmatrix} \bar{b}_2^{11} & \bar{b}_2^{12} \\ \bar{b}_2^{21} & \bar{b}_2^{22} \\ \bar{b}_2^{31} & \bar{b}_2^{32} \end{bmatrix}, \quad b_3 = \begin{bmatrix} 0 & 0 \\ 0 & 0 \\ \bar{b}_3^{31} & \bar{b}_3^{32} \end{bmatrix},$$

where the coefficients $\bar{a}_1^{11}, \bar{a}_2^{11}, \bar{b}_1^{11}, \bar{b}_1^{12}, \bar{b}_2^{11}, \bar{b}_2^{12}$, $\bar{a}_1^{22}, \bar{a}_2^{22}, \bar{b}_1^{21}, \bar{b}_1^{22}, \bar{b}_2^{21}, \bar{b}_2^{22}$ are 3rd-order polynomials of $p(k-2)$ and $\bar{a}_1^{33}, \bar{a}_2^{33}, \bar{a}_3^{33}, \bar{b}_1^{32}, \bar{b}_1^{31}, \bar{b}_2^{32}, \bar{b}_3^{32}, \bar{b}_3^{32}$ are 5th-order polynomials of $p(k-2)$, see (8). In the case of the LPV model with two scheduling variables, these coefficients are bivariate polynomials without the interaction terms. Therefore, the total number of the identified constant parameters are 96 and 172 for the LPV model with one- and two-scheduling variables, respectively.

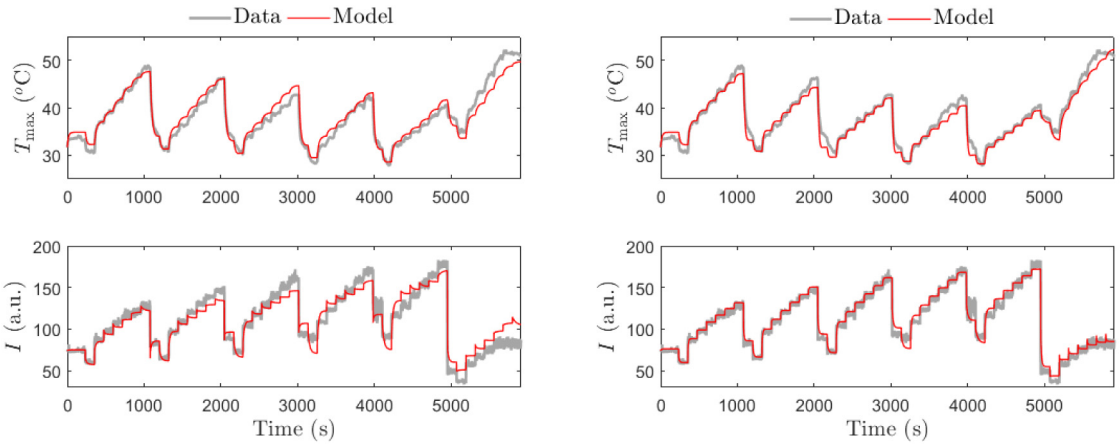

(a) LPV model with one scheduling variable (b) LPV model with two scheduling variables

Fig. 5. Predictions of the input–output LPV models with: (a) a single scheduling variable , and (b) two scheduling variables compared to an independent validation dataset. The outputs are the maximum temperature T_{max} and plasma optical intensity I.

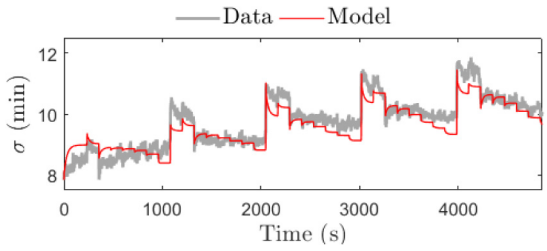

Fig. 6. Predictions of the input–output LPV model with two scheduling variables compared to an independent validation dataset. The output is the standard deviation of the surface temperature distribution σ.

Table 2
Specifications and tuning parameters of the LPV–MPC problem (19) for the real-time control experiments in Case I and Case II.

	Case I	Case II
N	5	5
Q	diag([5, 1])	diag([0.5, 1])
R	diag([0.1, 0.025])	diag([0.3, 3])
T_{max} (°C)	$(0, 45]$[a]	$(0, 45]$
I (a.u.)	$[10, \infty)$	$[10, \infty)$
q (slm)	[0.8, 5]	[0.8, 5]
P_{set} (W)	[1, 5]	[1, 5]

[a] T_{max} is constrained by $(0, 43]$ in the disturbance rejection case shown in Fig. 8.

5.2. Real-time control experiments

Once the LPV-IO models are identified, they are converted to the state–space form (17), as described in Section 4.2, and used to formulate the LPV–MPC problem (19). Two case studies are considered for the real-time control experiments: Case I — setpoint tracking in the presence of exogenous disturbances; and Case II — thermal dose delivery to a surface when the APPJ is stationary; see Section 3. The setpoints and constraints, as well as the tuning parameters, of the LPV–MPC problem for each case are summarized in Table 2.

Case I: Setpoint tracking for plasma optical intensity and maximum surface temperature

The control objective is to track time-varying setpoints for the maximum surface temperature T_{max} and plasma optical intensity I. Two LPV–MPC controllers are designed based on two LPV models that use a single and two scheduling variables, as described in Section 5.1. The LPV–MPC controllers are implemented on the APPJ via the hierarchical control strategy depicted in Fig. 2.

Fig. 7 shows the closed-loop performance of the control strategy for both LPV–MPC controllers. The real-time control experiments suggest that the increased complexity of the LPV model (i.e., including more scheduling variables) allows capturing the APPJ behavior more accurately, which results in an improved setpoint tracking performance. The LPV–MPC controller based on the LPV model with a single scheduled variable, i.e., setpoint to the embedded power controller P_{set}, leads to high-frequency oscillatory behavior in the inputs and outputs (Fig. 7(a)). In particular, it is difficult to adequately control the plasma optical intensity I with this controller. In contrast, the LPV–MPC controller based on two scheduling variables, i.e., P_{set} and He mass flow rate q, demonstrates an improved closed-loop tracking performance (Fig. 7(b)). In this case, the oscillatory behavior of the APPJ inputs is largely mitigated and the setpoint for the plasma optical intensity is tracked more effectively. Thus, the outputs under the LPV–MPC with two scheduling variables exhibit a smaller overshoot of their respective setpoints (less than 1 °C), while having a shorter settling time (c.f., time = 0 – 100 s in the temperature trajectories in Fig. 7) compared to the outputs under the LPV–MPC with one scheduling variable. Moreover, the setpoints have been attained very fast with maximum rise time of 9 and 2 samples for the temperature and the plasma intensity, respectively, with almost no steady-state errors. Furthermore, although both controllers generate control inputs that are within the desired input bounds (shown by the gray lines in Fig. 7), the LPV–MPC with a single scheduling variable leads to much more aggressive control actions. In practice, this can lead to actuator damage, which can be both dangerous and costly. Besides the more-aggressive nature of the control actions resulting from LPV–MPC with one scheduling variable, the manipulated inputs can also be seen to saturate frequently, which is a further indication of poor control performance.

The hierarchical control strategy based on LPV–MPC provides a significant advantage over the MPC strategy based on an LTI subspace identification model reported in Gidon et al. (2018). This is because the LPV–MPC controller allows exploiting a broader APPJ operating range by tracking a broader range of setpoint combinations for the tightly coupled outputs T_{max} and I. Similarly, the LPV–MPC controller can be expected to reject a broader range of disturbances acting on the APPJ. To test this, we investigate the ability of the controller in rejecting a disturbance in the jet tip-to-surface separation distance, which may routinely occur in the hand-held application of APPJs (e.g., for medical applications) or in treatment of surfaces with non-uniform topology. Variations in jet tip-to-surface separation distance

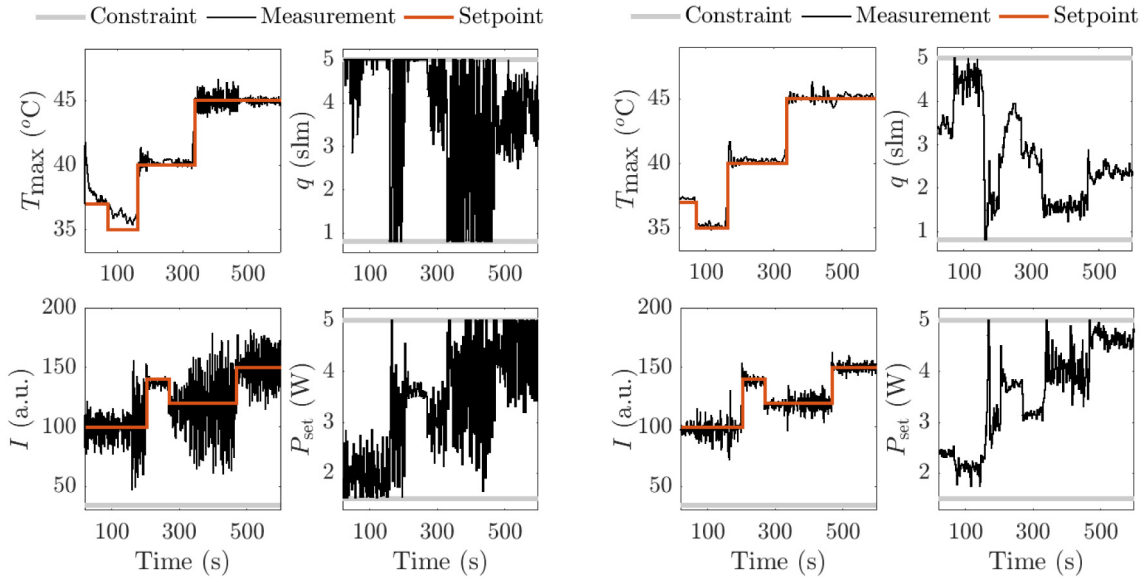

(a) LPV-MPC scheduled based on a single variable (b) LPV-MPC scheduled based on two variables

Fig. 7. Closed-loop performance of the hierarchical control strategy in Case I using LPV–MPC controllers scheduled based on: (a) one single scheduling variable, and (b) two scheduling variables. Controlled variables include maximum surface temperature T_{max} and plasma optical intensity I. Control inputs are the He flow rate q and setpoint to the embedded power controller P_{set}.

can drastically affect APPJ characteristics and their impacts on surfaces, including electric fields, delivered chemical species concentrations, and surface temperature (Breden & Raja, 2014; Gerling et al., 2012; Wu, Wand, Huang, Lu, & Pan, 2011). Thus, maintaining the APPJ characteristics in the presence of variations in jet tip-to-surface is key for reliable operation. Fig. 8 shows the closed-loop performance of the LPV–MPC controller scheduled with two variables in the presence of a step disturbance in APPJ tip-to-surface separation distance. The separation distance is increased from its nominal value of 4 mm up to 8 mm at $t = 80$ s and is returned to its original value of 4 mm at $t = 160$ s. The proposed control strategy demonstrates excellent performance in rejecting this disturbance, since it is able to track the setpoints in T_{max} and I with minimal deviation. This is in contrast to previous PI and MPC controllers tested on the same APPJ testbed, whereby both the surface temperature and plasma intensity deviate significantly from their setpoints, leading to constraint violations that are critical for the safe plasma treatment in medical applications (e.g., see Figure 7 in Gidon et al., 2018).

Case II: Thermal dose delivery with stationary APPJ

The control objective in this case is to deliver a thermal dose of $\text{CEM}_{\text{T}}^{\text{ref}} = 5$ min during a plasma treatment time of less than 5 min (see (1)). The thermal dose delivery problem is recast as a setpoint tracking problem in two steps: (i) the reference thermal dose $\text{CEM}_{\text{T}}^{\text{ref}}$ is converted to a setpoint tracking problem in terms of maximum surface temperature T_{max} using the soft sensor (4)–(5), and (ii) the spatial variation of dose delivery is regulated by tracking a setpoint for the standard deviation σ of the spatial distribution of the surface temperature. An LPV–MPC controller with two scheduling variables is designed, which is implemented on the APPJ using the hierarchical control strategy depicted in Fig. 3.

Fig. 9 shows the closed-loop performance of the proposed control strategy for regulating the thermal dose delivery. It is apparent that the setpoint for T_{max} is not tracked particularly well (see Fig. 9(a)). This is mainly a result of the weights assigned to T_{max} and σ in the control objective of the LPV–MPC problem (19); as listed in Table 2. Due to the tight coupling between σ and T_{max}, multivariable control of these two variables is particularly challenging. However, the temperature setpoint need not be tracked closely for the thermal dose delivery control

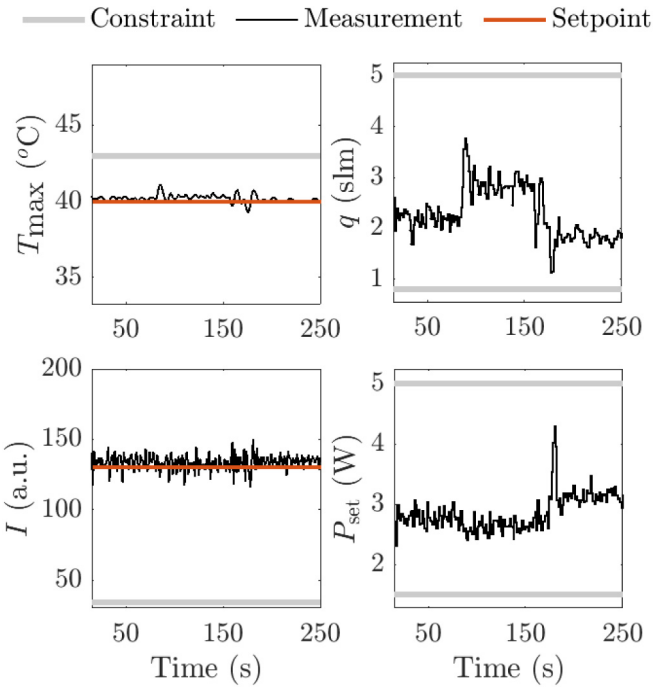

Fig. 8. Closed-loop performance of the hierarchical control strategy in Case I using the LPV–MPC controller scheduled based on two variables. The APPJ tip-to-surface separation distance (i.e., disturbance) is increased from 4 mm to 8 mm at $t = 80$ s and returned back to 4 mm at $t = 160$ s. Controlled variables include maximum surface temperature T_{max} and plasma optical intensity I. Control inputs are the He flow rate q and setpoint to the embedded power controller P_{set}.

objective. This is because the temperature setpoint is updated at each sampling time. Therefore, an offset at any particular time instant can be counteracted by choosing the setpoint appropriately in the next time instant(s). Here, we opted for a lower weight on T_{max}, as the soft sensor allows the T_{max} setpoint to be updated dynamically. Fig. 9(b) shows the temporal evolution and the final spatial distribution of the thermal

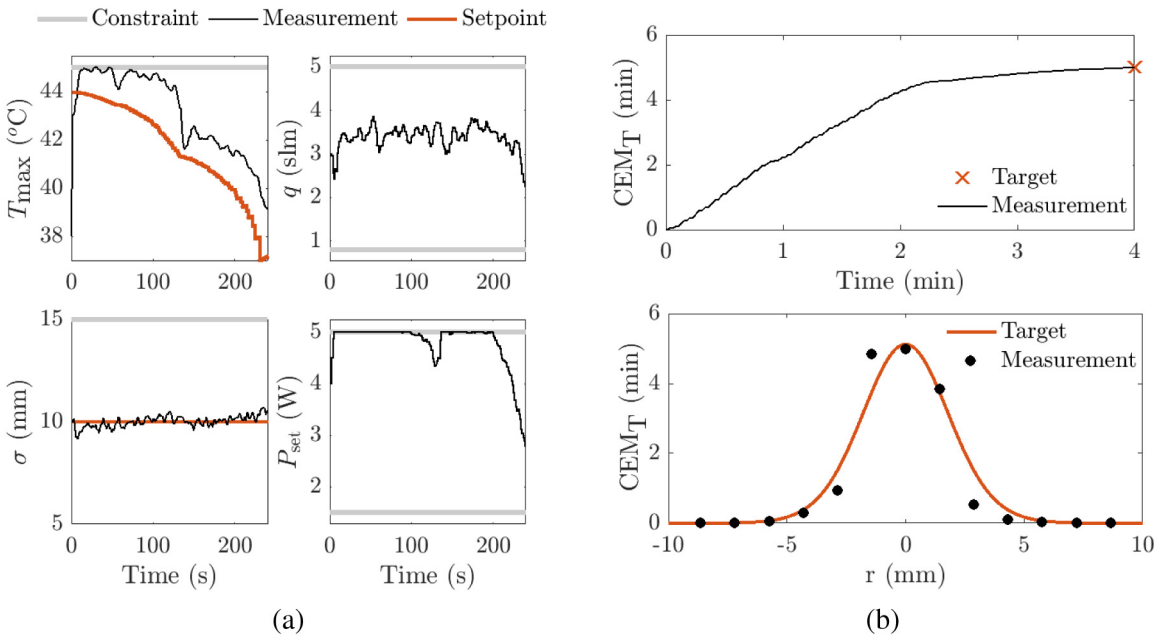

Fig. 9. Closed-loop performance of the hierarchical control strategy in Case II using the LPV–MPC controller scheduled based on two variables. (a) Controlled variables are maximum surface temperature T_{max} and standard deviation of the spatial distribution of the surface temperature σ, whereas control inputs are the He flow rate q and setpoint to the embedded power controller P_{set}. (b) Temporal evolution of the thermal dose CEM_T during the plasma treatment and the spatial dose distribution of CEM_T at the end of the treatment.

dose delivered to the surface. It can be seen that the reference thermal dose of $CEM_T^{ref} = 5$ min is achieved within the plasma treatment time. Despite the shortcomings in the setpoint tracking performance for T_{max}, the hierarchical control strategy allows T_{max} to be retained below its constraint, which can represent a critical safety consideration, for example, in medical applications of the APPJ (see Fig. 9(a)). This performance is comparable to the results reported in Gidon et al. (2017) (Figure 7), where a nonlinear lumped-parameter, physics-based model was used to model the thermal effects of the plasma on the surface. However, in Gidon et al. (2017) the nonlinear MPC is implemented in simulation only, and the underlying physics-based model suffered from restrictive assumptions. Therefore, this work provides experimental evidence for the effectiveness of MPC for thermal dose delivery using a nonlinear data-driven model.

Overall, the hierarchical control strategy based on the LPV–MPC controller is capable of delivering the target spatial distribution of the thermal dose CEM_T within the desired time of less than five minutes, as shown in Fig. 9(b). At the same time, the manipulated inputs to the APPJ, i.e., q and P_{set}, are not very oscillatory, thus circumventing the issues surrounding potential actuator damage discussed in the previous section. In addition, the He flow rate q does not reach its bounds, indicating that there is a lot of "margin" for flow rate actuation. However, the applied power P_{set} often saturates at its maximum value, indicating that for the intended application, a larger operating window for power may be needed. In practice, this may lead to plasma arcing, which is why a larger range for power was not examined in this study.

6. Conclusions

We presented a hierarchical control strategy based on a lower-level embedded power controller and a higher-level LPV–MPC controller for a kHz-excited APPJ in He. The adopted LPV modeling approach presented a convenient data-driven methodology, which allowed capturing the highly nonlinear behavior of the APPJ over a relatively broad operating range. The performance of the hierarchical control strategy based on the LPV–MPC was demonstrated in two cases: (i) setpoint tracking in the presence of disturbances; and (ii) thermal dose delivery when the APPJ is stationary. The real-time control experiments indicated the promise of data-driven modeling approaches in conjunction with MPC strategies for reproducible and effective operation of APPJs. The LPV–MPC with two scheduling variables yielded deviations from the temperature setpoint that are less than 1 °C (less than 0.5 °C in the case of disturbance rejection), while the desired thermal dose is delivered in 4 min. This is especially important in the context of plasma medicine, where treatment times are desired to be as short as possible to improve patient comfort. Future work will focus on investigating advanced learning approaches for data-driven LPV modeling and control of cold atmospheric plasmas.

Declaration of competing interest

The authors declare that they have no known competing financial interests or personal relationships that could have appeared to influence the work reported in this paper.

Appendix. Reformulation of optimal control problem as a quadratic programming problem

The optimal control problem (19) is recast as a quadratic programming problem as follows. The cost function can be rewritten as

$$J(k) = \frac{1}{2}\Delta U(k)^\top H \Delta U(k) + \Delta U(k)^\top f(k) + g(k), \tag{A.1}$$

where

$$H(k) = 2(\mathcal{R} + \mathcal{B}(k)^\top \mathcal{C}^\top \mathcal{Q}\mathcal{C}\mathcal{B}(k)),$$
$$f(k) = 2(\mathcal{B}(k)^\top \mathcal{C}^\top \mathcal{Q}\mathcal{C}\mathcal{A}(k)x(k) - \mathcal{B}(k)^\top \mathcal{C}^\top \mathcal{Q}Y_{set}(k)),$$

and $g(k)$ is a known scalar that can be omitted; the matrices $\mathcal{A}$, $\mathcal{B}$, $\mathcal{C}$, $\mathcal{Q}$, $\mathcal{R}$ and Y_{set} are given in Section 4. The set of constraints are now reformulated as

$$M(k)\Delta U(k) \leq b + L_u u(k-1) + L_x(k)x(k), \tag{A.2}$$

where

$$M(k) = \mathcal{E} + \mathcal{F}\Pi + \mathcal{G}\mathcal{B}(k), \quad L_u = -\mathcal{F}\mathcal{Y}, \quad L_x(k) = -\mathcal{G}\mathcal{A}(k),$$
$$b = \begin{bmatrix} -\Delta u_{min}^\top & \Delta u_{max}^\top & -u_{min}^\top & u_{max}^\top & -x_{min}^\top & x_{max}^\top \end{bmatrix}^\top,$$

with

$$\mathcal{E} = I_N \otimes \begin{bmatrix} -I_{n_u} \\ I_{n_u} \\ 0 \\ 0 \\ 0 \\ 0 \end{bmatrix}, \quad \mathcal{F} = I_N \otimes \begin{bmatrix} 0 \\ 0 \\ -I_{n_u} \\ I_{n_u} \\ 0 \\ 0 \end{bmatrix}, \quad \mathcal{G} = I_N \otimes \begin{bmatrix} 0 \\ 0 \\ 0 \\ 0 \\ -I_{n_x} \\ I_{n_x} \end{bmatrix},$$

$$\Pi = \begin{bmatrix} I_{n_u} & 0 & \cdots & 0 \\ I_{n_u} & I_{n_u} & \cdots & 0 \\ \vdots & \vdots & \ddots & \vdots \\ I_{n_u} & I_{n_u} & \cdots & I_{n_u} \end{bmatrix}, \quad \Upsilon = \begin{bmatrix} I_{n_u} \\ I_{n_u} \\ \vdots \\ I_{n_u} \end{bmatrix}.$$

Unlike conventional MPC for LTI systems, the cost function parameters H, f, g and the inequality constraint parameters M, L_x are time-varying in the LPV–MPC problem. Hence, they must be updated at every sampling time instant k.

References

Abbas, H. S., Ali, A., Hashemi, S. M., & Werner, H. (2014). LPV state-feedback control of a control moment gyroscope. *Control Engineering Practice*, *24*(3), 129–137.

Abbas, H. S., Hanema, J., Tóth, R., Mohammadpour, J., & Meskin, N. (2018). An improved robust model predictive control for linear parameter-varying input-output models. *International Journal of Robust and Nonlinear Control*, *28*(3), 859–880.

Arjunan, K. P., Obrusník, A., Jones, B. T., Zajíčková, L., & Ptasinska, S. (2016). Effect of additive oxygen on the reactive species profile and microbicidal property of a helium atmospheric pressure plasma jet. *Plasma Processes and Polymers*, *13*(11), 1087–1103.

Arora, D., Skliar, M., & Roemer, R. B. (2005). Minimum-time thermal dose control of thermal therapies. *IEEE Transactions on Biomedical Engineering*, *52*(2), 191–200.

Bachnas, A., Tóth, R., Ludlage, J., & Mesbah, A. (2014). A review on data-driven linear parameter-varying modeling approaches: A high-purity distillation column case study. *Journal of Process Control*, *24*(4), 272–285.

Bhoj, A. N., & Kushner, M. J. (2006). Multi-scale simulation of functionalization of rough polymer surfaces using atmospheric pressure plasmas. *Journal of Physics D: Applied Physics*, *39*(8), 1594.

Breden, D., & Raja, L. L. (2014). Computational study of the interaction of cold atmospheric helium plasma jets with surfaces. *Plasma Sources, Science and Technology*, *23*(6), Article 065020.

Casavola, A., Famularo, D., & Franzé, G. (0000). Predictive control of constrained nonlinear systems via LPV linear embeddings. *International Journal of Robust and Nonlinear Control*, 13(3–4), 281–294.

Dewhirst, M. W., Viglianti, B. L., Lora-Michiels, M., Hanson, M., & Hoopes, P. J. (2003). Basic principles of thermal dosimetry and thermal thresholds for tissue damage from hyperthermia. *International Journal of Hyperthermia*, *19*(3), 267–294.

Dünnbier, M., Schmidt-Bleker, A., Winter, J., Wolfram, M., Hippler, R., Weltmann, K.-D., et al. (2013). Ambient air particle transport into the effluent of a cold atmospheric-pressure argon plasma jet investigated by molecular beam mass spectrometry. *Journal of Physics D: Applied Physics*, *46*(43), Article 435203.

Gerber, I., Mihaila, I., Hein, D., Nastuta, A., Jijie, R., Pohoata, V., et al. (2017). Time behavior of helium atmospheric pressure plasma jet electrical and optical parameters. *Applied Sciences*, *7*(8), 812.

Gerling, T., Nastuta, A. V., Bussiahn, R., Kindel, E., & Weltmann, K.-D. K.-D. (2012). Back and forth directed plasma bullets in a helium atmospheric pressure needle-to-plane discharge with oxygen admixtures. *Plasma Sources, Science and Technology*, *21*(3), Article 034012.

Gidon, D., Curtis, B., Paulson, J. A., Graves, D. B., & Mesbah, A. (2018). Model-based feedback control of a kHz-excited atmospheric pressure plasma jet. *IEEE Transactions on Radiation and Plasma Medical Sciences*, *2*(2), 129–137.

Gidon, D., Graves, D. B., & Mesbah, A. (2017). Effective dose delivery in atmospheric pressure plasma jets for plasma medicine: A model predictive control approach. *Plasma Sources, Science and Technology*, *26*(8), 85005–85019.

Gidon, D., Graves, D. B., & Mesbah, A. (2019a). Predictive control of 2D spatial thermal dose delivery in atmospheric pressure plasma jets. *Plasma Sources, Science and Technology*, *28*(8), Article 085001.

Gidon, D., Graves, D. B., & Mesbah, A. (2019b). Spatial thermal dose delivery in atmospheric pressure plasma jets. *Plasma Sources, Science and Technology*, *28*, Article 025006.

Keidar, M., Yan, D., & Sherman, J. H. (2019). Adaptive plasmas and recent progress in plasma application in cancer therapy. In *Cold plasma cancer therapy (vol. 2053–2571)* (pp. 7–1 to 7–9). Morgan & Claypool Publishers.

Laroussi, M., Kong, M., Morfill, G., & Stolz, W. (2012). *Plasma medicine*. Cambridge University Press.

Laurain, V., Gilson, M., Tóth, R., & Garnier, H. (2010). Refined instrumental variable methods for identification of LPV Box–Jenkins models. *Automatica*, *46*(6), 959–967.

Lee, H., Park, G., Seo, Y., Im, Y., Shim, S., & Lee, H. (2011). Modelling of atmospheric pressure plasmas for biomedical applications. *Journal of Physics D: Applied Physics*, *44*(5), Article 053001.

Ljung, L. (1999). *System identification, theory for the user* (2nd ed.). USA: Prentice-Hall Inc., ISBN: 0-13-656695-2.

Mani, M., Lane, B., Donmez, A., Feng, S., Moylan, S., & Fesperman, R. (2015). *Measurement science needs for real-time control of additive manufacturing powder bed fusion processes*: *Tech. rep.*, National Institute of Standards and Technology.

Mesbah, A., & Graves, D. B. (2019). Machine learning for modeling, diagnostics, and control of non-equilibrium plasmas. *Journal of Physics D: Applied Physics*, *52*(30), Article 30LT02.

Metelmann, H. R., Seebauer, C., Rutkowski, R., Schuster, M., Bekeschus, S., & Metelmann, P. (2018). Treating cancer with cold physical plasma: On the way to evidence-based medicine. *Contributions to Plasma Physics*, *58*(5), 1–5.

Mohammadpour, J., & Scherer, C. (2012). *Control of linear parameter varying systems with applications*. New York: Springer-Verlag.

Morent, R. (2013). Editorial: Atmospheric pressure plasma polymerization. *The Open Plasma Physics Journal*, *7*(1), 6.

Norberg, S. A., Johnsen, E., & Kushner, M. J. (2015). Helium atmospheric pressure plasma jets touching dielectric and metal surfaces. *Journal of Applied Physics*, *118*(1), 1–13.

Rawlings, J. B., & Mayne, D. Q. (2009). *Model predictive control: Theory and design*. Nob Hill Pub.

Rizvi, S. Z., Velni, J. M., Abbasi, F., Tóth, R., & Meskin, N. (2018). State-space LPV model identification using kernelized machine learning. *Automatica*, *88*, 38–47.

Rugh, W. J., & Shamma, J. S. (2000). Research on gain scheduling. *Automatica*, *36*, 1401–1425.

Schmidt-Bleker, A., Winter, J., Bösel, A., Reuter, S., & Weltmann, K.-D. (2016). On the plasma chemistry of a cold atmospheric argon plasma jet with shielding gas device. *Plasma Sources, Science and Technology*, *25*(1), Article 015005.

Shin, J., & Raja, L. L. (2007). Run-to-run variations, asymmetric pulses, and long time-scale transient phenomena in dielectric-barrier atmospheric pressure glow discharges. *Journal of Physics D: Applied Physics*, *40*(10), 3145–3154.

Tóth, R. (2010). *Modeling and identification of linear parameter-varying systems*. Berlin, Heidelberg: Springer–Verlag.

Tóth, R., Abbas, H. S., & Werner, H. (2012). On the state-space realization of LPV input-output models: Practical approaches. *IEEE Transactions on Control Systems Technology*, *20*(1), 139–153.

Van Dijk, J., Kroesen, G., & Bogaerts, A. (2009). Plasma modelling and numerical simulation. *Journal of Physics D: Applied Physics*, *42*(19), Article 190301.

Van Overschee, P., & De Moor, B. L. (2012). *Subspace identification for linear systems: Theory—Implementation—Applications*. Springer Science & Business Media.

von Woedtke, T., Metelmann, H.-R., & Weltmann, K.-D. (2014). Clinical plasma medicine: State and perspectives of in vivo application of cold atmospheric plasma. *Contributions to Plasma Physics*, *54*(2), 104–117.

Wu, S., Wand, Z., Huang, Q., Lu, X., & Pan, Y. (2011). Study on a room-temperature air plasma for biomedical application. *IEEE Transactions on Plasma Science*, *39*(6), 1489–1495.